

Excited-state quantum phase transitions in the anharmonic Lipkin-Meshkov-Glick model: Static aspects


J. Gamito ¹, J. Khalouf-Rivera ², J. M. Arias ^{1,3}, P. Pérez-Fernández ^{3,4} and F. Pérez-Bernal ^{2,3}

¹*Departamento de Física Atómica, Molecular y Nuclear, Facultad de Física, Universidad de Sevilla, Apartado 1065, 41080 Sevilla, Spain*

²*Departamento de Ciencias Integradas y Centro de Estudios Avanzados en Física, Matemáticas y Computación, Universidad de Huelva, Huelva 21071, Spain*

³*Instituto Carlos I de Física Teórica y Computacional, Universidad de Granada, Fuentenueva s/n, 18071 Granada, Spain*

⁴*Departamento de Física Aplicada III, Escuela Técnica Superior de Ingeniería, Universidad de Sevilla, 41092 Sevilla, Spain*

 (Received 10 March 2022; revised 20 July 2022; accepted 15 August 2022; published 17 October 2022)

The basic Lipkin-Meshkov-Glick model displays a second-order ground-state quantum phase transition and an excited-state quantum phase transition (ESQPT). The inclusion of an anharmonic term in the Hamiltonian implies a second ESQPT of a different nature. We characterize this ESQPT using the mean field limit of the model. The alternative ESQPT, associated with the changes in the boundary of the finite Hilbert space of the system, can be properly described using the order parameter of the ground-state quantum phase transition, the energy gap between adjacent states, the participation ratio, and the quantum fidelity susceptibility.

DOI: [10.1103/PhysRevE.106.044125](https://doi.org/10.1103/PhysRevE.106.044125)

I. INTRODUCTION

Ground-state quantum phase transitions (QPTs), zero-temperature transitions that are triggered by quantum fluctuations instead of thermal ones, have been in the limelight in recent years due to their deep implications in the understanding of many-body quantum systems [1]. In these transitions the ground state of the system undergoes abrupt and qualitative changes when one or several control parameters in the Hamiltonian straddle a critical value. Since the seminal works of Gilmore and co-workers [2–4], there have been numerous works characterizing QPTs in two-level quantum systems of different dimensionality used to model nuclear and molecular systems, such as the interacting boson model (IBM) or the vibron model (see Refs. [5–7] and references therein). A full classification of ground-state QPTs in two-level models with different dimensionality can be found in Ref. [8].

The study of QPTs has been extended to the realm of excited states, introducing the concept of excited-state quantum phase transition (ESQPT) which implies a nonanalyticity in the density of states and the energy level flow which, in most cases, is associated with a ground-state QPT and the existence of a critical point in the energy functional obtained from the classical or mean field limit of the system [9–11]. The nature of the nonanalyticity in the energy level density in nondegenerate stationary points of systems with n effective degrees of freedom is such that the order of the derivative of the level density that is nonanalytic is $n - 1$ [11–15]. Excited-state quantum phase transitions have received a great deal of attention in many systems, fostered by detection of their precursors in molecular spectra [16–19], superconducting microwave billiards [20], and spinor condensates [21]. In the last case, some promising developments have

been recently published [22,23]. Reference [24] is a review on different aspects of ESQPTs with an extensive reference list.

A system where ESQPTs have been studied is the two-dimensional limit of the vibron model (2DVM), a two-level model built upon the bilinear products of two Cartesian operators and a scalar bosonic operator [25,26]. This model has been used to reproduce bending spectra of molecules, as its two dynamical symmetries can be associated with the bending degrees of freedom for linear and bent molecular species, as well as the interesting situations that lie in between these two limiting cases [27,28]. The basic 2DVM Hamiltonian, including only a number and a pairing operator, presents a second-order ground-state QPT and an associated ESQPT that can be linked to the effect over excited energy levels of the barrier to linearity in nonrigid molecular systems [26]. In fact, most experimental ESQPT signatures that were identified in the bending degrees of freedom of nonrigid molecules are associated with this ESQPT [16,17,19]. The obtention of results of spectroscopic quality in the modeling of molecular spectra implies the explicit inclusion of anharmonic terms in the 2DVM Hamiltonian. In Ref. [29] it was shown that the inclusion of anharmonicity in the Hamiltonian results in a second ESQPT in the broken-symmetry phase, which is where the typical spectroscopic signatures of nonrigid molecules are found. More recently, in the pursuit of the description of the transition state in isomerization reactions [18], it has been found that the second ESQPT can also be present in the symmetric phase for sufficiently large values of the anharmonicity and it is not associated with the ground-state QPT but it stems from changes in the phase-space boundary of the 2DVM's finite-dimensional Hilbert space [30].

A particular kind of such ESQPTs has been already studied in matter-radiation interaction models with two degrees of

freedom (Dicke and Tavis-Cummings models). In this case, the authors referred to these ESQPTs happening at the boundary of the model space as static ESQPTs, due to their lack of effect on the system dynamics. In this way, they can be distinguished from the more usual ESQPTs, which the authors refer to as dynamic ESQPTs [31]. More information on ESQPTs associated with the finiteness of the system Hilbert space can be found in Refs. [15,24].

Our aim is to extend the results obtained for the 2DVM [29,30] to the Lipkin-Meshkov-Glick (LMG) model. This model was introduced as a toy model for interacting fermions in nuclear physics, to help assess the performance of different approximations used in the study of nuclear structure [32–34]. It can be mapped to a set of spins with a long-range all-to-all interaction, and from their initial purpose it was later used in many different contexts. In particular, it was extensively used for the study of QPTs [35–45] and ESQPTs [46–55]. The general LMG model presents first-, second-, and third-order ground-state QPTs [43], something that has attracted the interest of researchers. In a basic formulation, with a Hamiltonian composed of two operators that can be mapped to a number and a pairing operator, the model has a second-order ground-state QPT and its associated ESQPT. A particular realization of the LMG model has a classical limit energy functional that is equal to classical limit of the IBM and it has been used as a tool to shed light upon QPTs and ESQPTs in this model [56–58]. It is also a toy model that can be applied in quantum computing [59–61]. The interest in the LMG model was further fostered by the achievement of different experimental realizations, using molecular magnets [62], optical cavities [63], Bose-Einstein condensates [64], nuclear magnetic resonance systems [65], trapped atoms [66–68], and cold atoms [69].

The purpose of the present article is to explore how the LMG model is modified, including in the model Hamiltonian the anharmonic two-body term $\hat{n}(\hat{n} + 1)$ with a negative control parameter α . We perform a mean field analysis of the anharmonic LMG model, characterize ground-state QPT in this case, and perform a study of the two ESQPTs that appear in the model making use of different quantities such as the energy gap between adjacent levels, the ground-state QPT order parameter, the participation ratio, and the quantum fidelity susceptibility. This paper will be followed by another one that focuses on the effect of the two ESQPTs on dynamical properties of the model [70].

The present paper is organized as follows. In Sec. II we introduce the anharmonic LMG model, review its algebraic structure, provide its Hamiltonian matrix elements, and study the model mean field or thermodynamic limit using the coherent state formalism. Section III includes a description of the different quantities used to characterize the anharmonic LMG ESQPTs and the results obtained for different anharmonicity and system-size values. We summarize in Sec. IV.

II. MODEL

The LMG model has recently been attracting increasing attention after the experimental realization of one-dimensional spin- $\frac{1}{2}$ lattices with a variable interaction range [66,71]. Using

Pauli spin matrices $\sigma_{i,\beta}$, with $i = 1, 2, \dots, N$ and $\beta = x, y, z$, the system Hamiltonian is

$$\hat{H}^{(a)} = B \sum_{i=1}^N \sigma_{i,z} + \sum_{i < j=1}^N \frac{K}{|i-j|^a} \sigma_{i,x} \sigma_{j,x}, \quad (1)$$

where we assume $\hbar = 1$, B is the amplitude of an external magnetic field, K is the energy scale of the interactions between different spin sites, and the parameter a controls the interaction range. For $a = 0$ the interaction range is infinite and the Hamiltonian (1) is mapped to the LMG model [32–34]

$$\hat{H} = \hat{H}^{(a=0)} = (1 - \xi)(S + \hat{S}_z) + \frac{2\xi}{S}(S^2 - \hat{S}_x^2), \quad (2)$$

where we introduce collective spin operators $\hat{S}_\beta = \frac{1}{2} \sum_{i=1}^N \sigma_{i,\beta}$ for $\beta = x, y, z$, add a constant term $2BS - KS(2S - 1)$, and define a single control parameter ξ , making $2B = 1 - \xi$ and $SK = -\xi$. The control parameter is defined in the range $\xi \in [0, 1]$, driving the system from one phase to the other one. Indeed, from an algebraic point of view, the LMG Hamiltonian given by Eq. (2) presents a $u(2)$ algebraic structure, with two limiting dynamical symmetries: $u(2) \supset u(1)$ and $u(2) \supset so(2)$. Each dynamical symmetry is associated with a different phase. For $\xi = 1$, the Hamiltonian is diagonal in the basis associated with the $so(2)$ subalgebra and this is known as the deformed or broken-symmetry phase; in contrast, for $\xi = 0$ the Hamiltonian is diagonal in the $u(1)$ subalgebra basis and it is in the normal or symmetric phase [72]. The LMG model Hamiltonian (2) experiences a second-order ground-state QPT at the critical value of the control parameter $\xi_c = 0.2$ [43].

Inspired by the work in Refs. [29,30], we include in the Hamiltonian (2) an anharmonic term, using a second-order operator on \hat{S}_z ,

$$\hat{H}_{\text{anh}} = (1 - \xi)(S + \hat{S}_z) + \frac{\alpha}{2S}(S + \hat{S}_z)(S + \hat{S}_z + 1) + \frac{2\xi}{S}(S^2 - \hat{S}_x^2). \quad (3)$$

The new Hamiltonian still depends on the control parameter ξ , which drives the system between phases, but it also depends on a second control parameter α . For $\alpha = 0$, we recover the original Hamiltonian (2), and for α values different from zero, the $\xi = 0$ limit is transformed from a truncated one-dimensional harmonic oscillator to an anharmonic oscillator. That is the reason why we refer to the Hamiltonian (3) as the anharmonic LMG (ALMG) model. It is worth noting that the limit $so(2)$ is no longer recovered for $\xi = 1$, unless $\alpha = 0$. In Ref. [73], a preliminary study of an anharmonic LMG model using only operators diagonal in the $u(1)$ basis was carried out.

The Hilbert space for the Hamiltonian (1) has dimension 2^N , but in the long-range interaction (3) there is a drastic reduction in the dimension of the Hilbert space due to the conservation of the total spin $[\hat{S}^2, \hat{H}] = 0$. We focus on the sector that corresponds to the maximum angular momentum $S = N/2$, with a Hilbert space dimension $N + 1$.

In the ALMG model, as in the original LMG model, there are two bases available to carry out the calculations, one

defined by the $u(2) \supset u(1)$ dynamical algebra, $|S, M_z\rangle$, where $M_z = -S, \dots, 0, \dots, S$ is the projection of the total spin S in

the z direction. The matrix elements of the Hamiltonian (3) in the $u(1)$ basis are

$$\begin{aligned} \langle S, M'_z | \hat{H}_{\text{anh}} | S, M_z \rangle = & \left\{ (1 - \xi)(S + M_z) + \frac{\xi}{2S} [4S^2 - (S - M_z)(S + M_z + 1) - (S + M_z)(S - M_z + 1)] \right. \\ & \left. + \frac{\alpha}{2} \left[S + 1 + \left(2 + \frac{1}{S} \right) M_z + \frac{M_z^2}{S} \right] \right\} \delta_{M'_z, M_z} \\ & - \frac{\xi}{2S} \sqrt{(S - M_z)(S - M_z - 1)(S + M_z + 2)(S + M_z + 1)} \delta_{M'_z, M_z + 2}. \end{aligned} \quad (4)$$

As can be easily seen from the matrix elements in Eq. (4), only states with $M'_z = M_z$ or $M'_z = M_z \pm 2$ are connected; hence the ALMG Hamiltonian (3) conserves parity $(-1)^{S+M_z}$ and the Hamiltonian matrix is split into two blocks, one for positive or even parity and dimension $S + 1$ and the other for negative or odd parity with dimension S . The second basis is associated with the $u(2) \supset so(2)$ symmetry $|S, M_x\rangle$, and in this case it is the projection of the spin in the x direction, the second quantum label in the basis. The matrix elements in this case can be deduced from the previous ones once the system is rotated [72].

We depict in Fig. 1 the correlation energy diagram for the ALMG Hamiltonian (3) with a system size $N = 2S = 120$ and $\alpha = 0$ and -0.6 in Figs. 1(a) and 1(b), respectively. In both cases, we plot the normalized excitation energy as a function of the control parameter ξ . Both positive- and negative-parity states are included in the figure; positive-parity energy levels are plotted with blue solid lines and odd-parity states with red dashed lines. Figure 1(a) shows clearly the ground-state QPT at $\xi_c = 0.2$ and the separatrix, marked by a high density of states, which is the boundary between the two ESQPT phases. Excited states above the separatrix have a $u(1)$ (symmetric) character, while those below it have an $so(2)$ (broken symmetry) character. It can be appreciated in the figure how beyond the critical value of the control parameter ξ and for states under the separatrix, the even- and odd-parity states are degenerated. From this figure it is already clear that the new ESQPT is not a static ESQPT using the notation introduced in Ref. [31]. In the present case, as it is confirmed in the semiclassical analysis in the next section, the nonanalyticity of the density of states is of the same kind in the two ESQPTs and both have noticeable effects on the system dynamics [70].

Figure 1(b) is the correlation energy diagram for a negative α value. As expected from the results obtained for the two-dimensional limit of the vibron model [29,30], there is a new separatrix that crosses the one associated with the ground-state QPT and the degeneracy pattern is more complex. In order to better understand the second separatrix we study the classical limit of the model, making use of the spin coherent states formalism [74].

Classical limit of the model

The classical limit of the Hamiltonian (3) can be obtained within a mean field analysis, studying the large-size limit of the model. We perform this study using spin coherent states

[74]. From the usual definitions and using the notation introduced in the preceding section, the spin ladder operators are $\hat{S}_{\pm} = \hat{S}_x \pm i\hat{S}_y$ and the spin coherent state is defined as

$$\begin{aligned} |[S]\mu\rangle &= \frac{\exp(\mu\hat{S}_+)}{(1 + |\mu|^2)^S} |S, -S\rangle \\ &= \frac{1}{(1 + |\mu|^2)^S} \sum_{p=0}^{2S} \sqrt{\binom{2S}{p}} \mu^p |S, -S + p\rangle, \end{aligned} \quad (5)$$

where μ is a complex parameter that encompasses the classical position and momentum variables, $|S, -S + p\rangle$ is a eigenstate of \hat{S}_z , $\hat{S}_z |S, -S + p\rangle = (-S + p) |S, -S + p\rangle$, and $(\hat{S}_+)^p |S, -S\rangle = \sqrt{\frac{p!(2S)!}{(2S-p)!}} |S, -S + p\rangle$ [74]. The expectation value of the operators \hat{S}_z , \hat{S}_+ , and \hat{S}_- with the spin coherent state (5) are

$$\begin{aligned} \langle [S]\mu | \hat{S}_z | [S]\mu \rangle &= S \frac{|\mu|^2 - 1}{|\mu|^2 + 1}, \\ \langle [S]\mu | \hat{S}_+ | [S]\mu \rangle &= S \frac{2\mu^*}{|\mu|^2 + 1}, \\ \langle [S]\mu | \hat{S}_- | [S]\mu \rangle &= S \frac{2\mu}{|\mu|^2 + 1}. \end{aligned} \quad (6)$$

Thus, the classical limit of the ALMG model, $H_{\text{cl}}(\mu)$, can be obtained as the expectation value of the Hamiltonian (3) (per particle) with the coherent state in the large-system-size limit ($S \rightarrow \infty$)

$$\begin{aligned} H_{\text{cl}}(\mu) &= \frac{\langle [S]\mu | \hat{H}_{\text{anh}} | [S]\mu \rangle}{2S} \\ &= (1 - \xi) \frac{|\mu|^2}{1 + |\mu|^2} + \alpha \left(\frac{|\mu|^2}{1 + |\mu|^2} \right)^2 \\ &\quad + \xi \left[1 - \left(\frac{\mu + \mu^*}{1 + |\mu|^2} \right)^2 \right], \end{aligned} \quad (7)$$

where the complex variable μ can be mapped into (q, p) (the canonical coordinate and momentum) by

$$q = \frac{1}{\sqrt{2}} \frac{\mu + \mu^*}{\sqrt{1 + |\mu|^2}}, \quad (8)$$

$$p = \frac{-i}{\sqrt{2}} \frac{(\mu - \mu^*)}{\sqrt{1 + |\mu|^2}}. \quad (9)$$

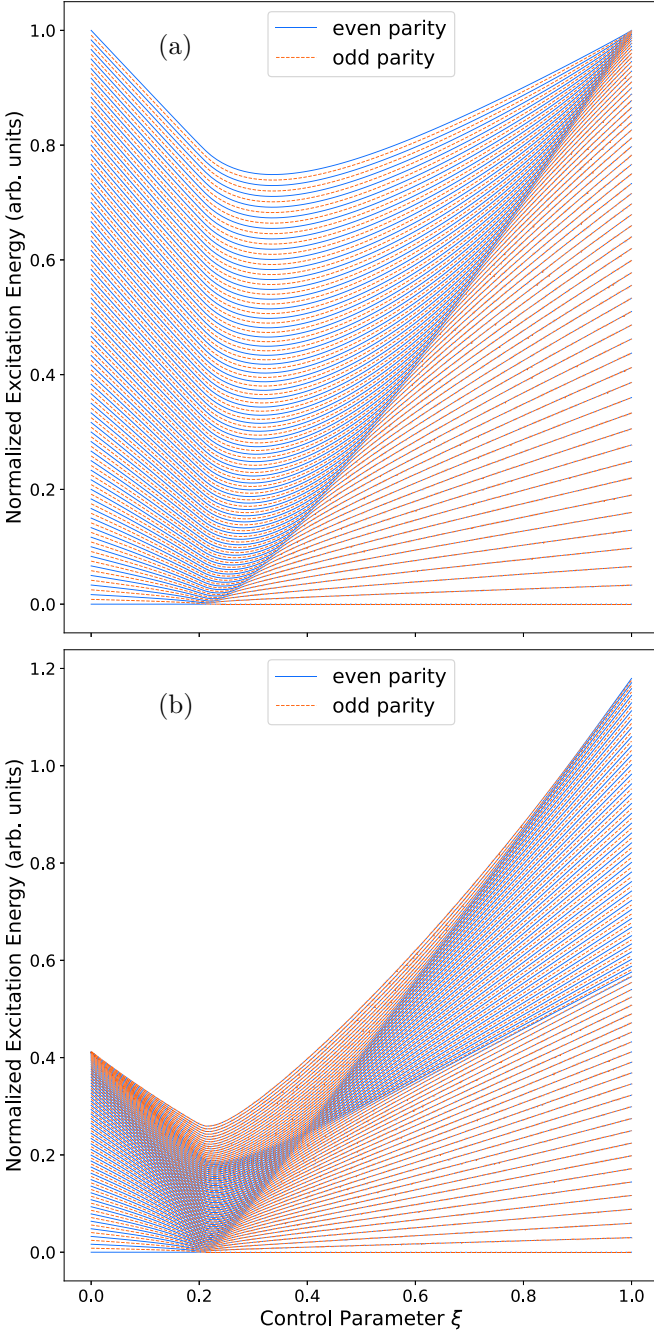


FIG. 1. Correlation energy diagram depicting the normalized excitation energies for even (blue solid lines) and odd (red dashed lines) parity states as a function of the control parameter $\xi \in [0, 1]$ for a system with size $N = 120$ and anharmonicity parameter (a) $\alpha = 0$ and (b) -0.6 .

Applying this transformation, the resulting classical Hamiltonian is

$$H_{\text{cl}}(q, p) = \frac{1-\xi}{2}(p^2 + q^2) + \frac{\alpha}{4}(p^2 + q^2)^2 + \xi q^2(p^2 + q^2 - 2) + \xi. \quad (10)$$

The resulting energy functional should provide the functional form of the separatrices that mark the critical ESQPT energies in Fig. 1, one in the $\alpha = 0$ case [Fig. 1(a)] and two

for $\alpha < 0$ [Fig. 1(b)]. The separatrix starting at the critical value of the control parameter $\xi_c = 0.2$ has been already characterized for $\alpha = 0$. We present results for both ESQPTs with a special focus on the anharmonicity-related critical line, exploring whether this line has the same nature and implications as the other and to what extent it has an impact in the system structure. The changes in the system dynamics associated with the introduction of the anharmonicity in the LMG model are explored in [70].

Assuming $\xi \in [0, 1]$ and $\alpha < 0$, the critical or stationary points of the Hamiltonian, where the first derivatives of Eq. (10) are zero, are

$$\frac{\partial H_{\text{cl}}(q, p)}{\partial q} = 0 \quad \rightarrow \quad \begin{cases} (q_0^2 = 0, p_0^2 = 0) \\ (q_1^2 = \frac{5\xi-1}{4\xi+\alpha}, p_1^2 = 0) \\ (q_2^2 = \frac{\xi-1-2\alpha}{2\xi}, p_2^2 = \frac{1+2\alpha+3\xi}{2\xi}) \\ (q_3^2 = 0, p_3^2 = \frac{\xi-1}{\alpha}). \end{cases} \quad (11)$$

According to the classical limit, the origin is a stationary point and it corresponds to the system ground state in the control parameter range $\xi \in [0, \xi_c]$ where the critical point is $\xi_c = 0.2$. For values of the control parameter $\xi \in (\xi_c, 1]$, the minimum energy is attained for the (q_1, p_1) coordinate and momentum values. In this way, the system ground-state energy as a function of the control parameters can be expressed as

$$E_{\text{gs}}(\xi, \alpha) = \begin{cases} \xi, & \xi \leq 0.2 \\ \frac{-1+\xi(10+4\alpha-9\xi)}{4(\alpha+4\xi)}, & \xi > 0.2. \end{cases} \quad (12)$$

From this equation is clear that the Hamiltonian (3) in the mean field limit has a critical point at $\xi_c = 0.2$, where the second derivative of the ground-state energy with respect to the control parameter ξ is discontinuous. This is in good agreement with the results obtained in [8] for a Hamiltonian including one- and two-body operators. Hence, the crossing of this critical point is marked by a second-order ground-state QPT. The energy gap vanishes and the ground state becomes parity degenerated. In addition to this and in a way similar to other systems with a transition between $u(n)$ and $so(n+1)$ dynamical symmetries [26], an ESQPT appears at an energy $H_{\text{cl}}(q_0, p_0) = \xi$. The critical excitation energy of the ESQPT defines the separatrix with a high density of states shown in Fig. 1. An analytical expression for this separatrix can be computed as

$$f_1(\xi, \alpha) = H_{\text{cl}}(q_0, p_0) - H_{\text{cl}}(q_1, p_1) = \frac{(1-5\xi)^2}{4(4\xi+\alpha)} \quad (13)$$

for $\xi \in (\xi_c, 1]$.

For negative α values there can be a second separatrix in this system, as shown in Fig. 1(b). When the condition $\alpha < (\xi - 1)/2$ is satisfied, the second ESQPT appears at a critical energy $H_{\text{cl}}(q_2, p_2) = 1 + \alpha$. The excitation energy for this new ESQPT marks the second separatrix in Fig. 1(b) and can be computed as

$$f_2(\xi, \alpha) = \begin{cases} H_{\text{cl}}(q_2, p_2) - H_{\text{cl}}(q_0, p_0) = 1 + \alpha - \xi, & \xi \leq \xi_c \\ H_{\text{cl}}(q_2, p_2) - H_{\text{cl}}(q_1, p_1) = \frac{(1+2\alpha+3\xi)^2}{4(\alpha+4\xi)}, & \xi > \xi_c. \end{cases} \quad (14)$$

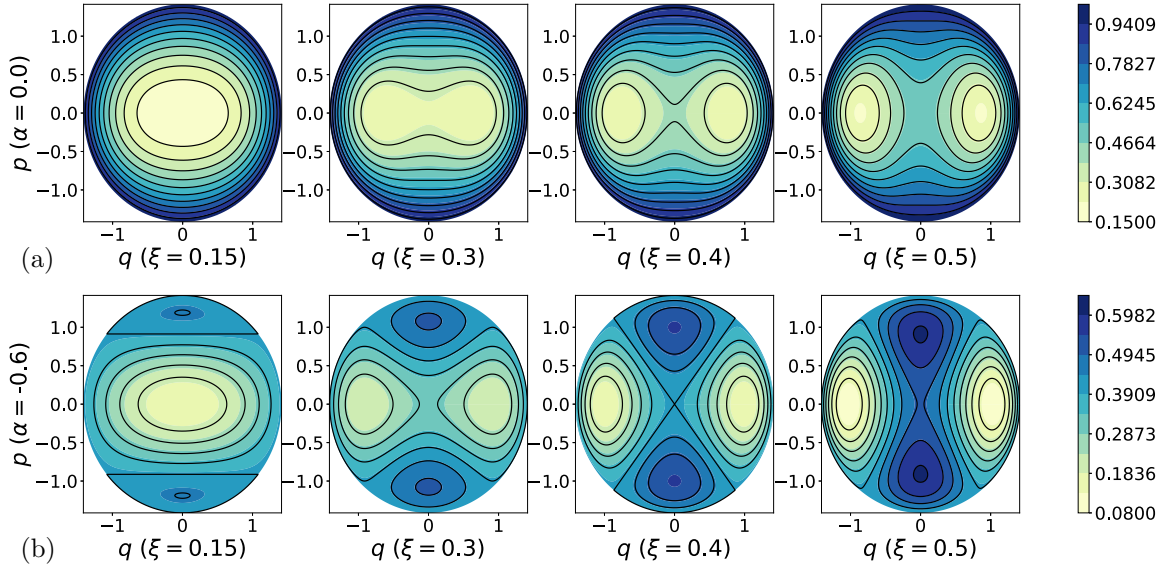


FIG. 2. Contour plots of the classical Hamiltonian (10) for systems with (a) $\alpha = 0.0$ and (b) $\alpha = -0.6$ and different values of the control parameter, from left to right: $\xi = 0.15, 0.3, 0.4$, and 0.5 . Each row shares the scale (right color axes).

As previously mentioned, a similar ESQPT in the broken-symmetry phase of the two-dimensional limit of the vibron model was studied in Ref. [29] and it was recently shown to be present in the symmetric phase of the model too [30].

In the symmetric phase $\xi \in [0, \xi_c]$, pair of eigenstates with different parities are degenerate for energies above the $f_2(\xi, \alpha)$ separatrix. In the broken-symmetry phase $\xi \in (\xi_c, 1]$, both separatrices can coexist and the pairs of eigenvalues with even and odd parities are degenerate below and above both of them and nondegenerate in between the two separatrices. This is shown clearly in Fig. 1(b). The critical point (q_3, p_3) marks the largest energy of the system, $H_{cl}(q_3, p_3) = \frac{-1+(2+4\alpha-\xi)\xi}{4\alpha}$, if the solution (q_2, p_2) exists. In fact, taking this into account and equating $H_{cl}(q_2, p_2) = H_{cl}(q_3, p_3)$, the threshold value of α in order that the second ESQPT exists can be obtained as $\alpha_{th}(\xi) = (\xi - 1)/2$. From this equation it is clear that the second ESQPT is present not only in the broken-symmetry phase, but also in the symmetric phase. This was recently discussed for a different model, the 2DVM [30], and it is a clear example of an ESQPT without an associated QPT, something that usually happens in systems with more than one control parameter for some trajectories in the parameter space [75–77]. In this case, the situation is somewhat different and the second ESQPT can be associated with changes in the boundaries in the finite Hilbert space of the system [15,24,31].

In Fig. 2 we show the contour plot of the classical Hamiltonian (10) for two different values of the anharmonic interaction, one without the f_2 (ESQPT (14), with $\alpha = 0.0$ [Fig. 2(a)]) and another with a value of the control parameter smaller than the threshold, $\alpha = -0.6$ [Fig. 2(b)]. In both cases different values of the control parameter ξ have been studied, from left to right $\xi = 0.15, 0.3, 0.4$, and 0.5 . The cases with $\alpha = 0.0$ present one minimum for $\xi < 0.2$ and two minima in the broken-symmetry phase [Fig. 2(a)]. In the four examples the maximum values of the energy correspond to $q_2^2 + p_2^2 = 2$. When the control parameter α takes a value smaller than the threshold [Fig. 2(b)], two maxima appear for $q_3 = 0$ and

$p_3 \neq 0$, which correspond to the new system limit. In these cases, systems present a new ESQPT due to the system limit $q_2^2 + p_2^2 = 2$.

In order to check the threshold value $\alpha_{th}(\xi)$, we have computed the maximum excitation energy for different values of α and system sizes and we have fit the maximum normalized excitation energy to a functional form $E_{max} = E_{cl} + cN^{-b}$ for a constant $\xi = \xi_c$. The resulting values of E_{cl} for ξ_c and various values of α are a good estimate of the maximum excitation energy of the system in the classical limit. The difference between E_{cl} and the separatrix $f_2(\xi_c, \alpha)$ is depicted in Fig. 3,

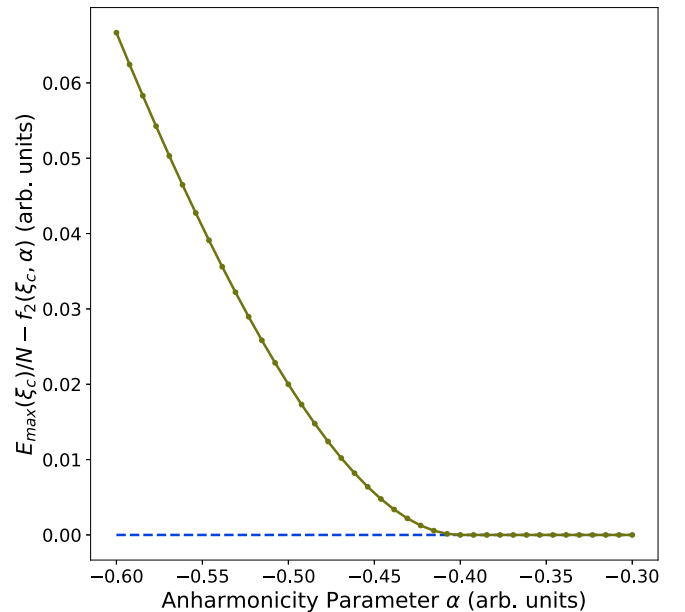


FIG. 3. The olive green solid line is the difference between the maximum normalized excitation energy of the ALMG (see the text for details) and the separatrix (14) for $\xi = \xi_c = 0.2$. The horizontal blue dashed line marks the zero value.

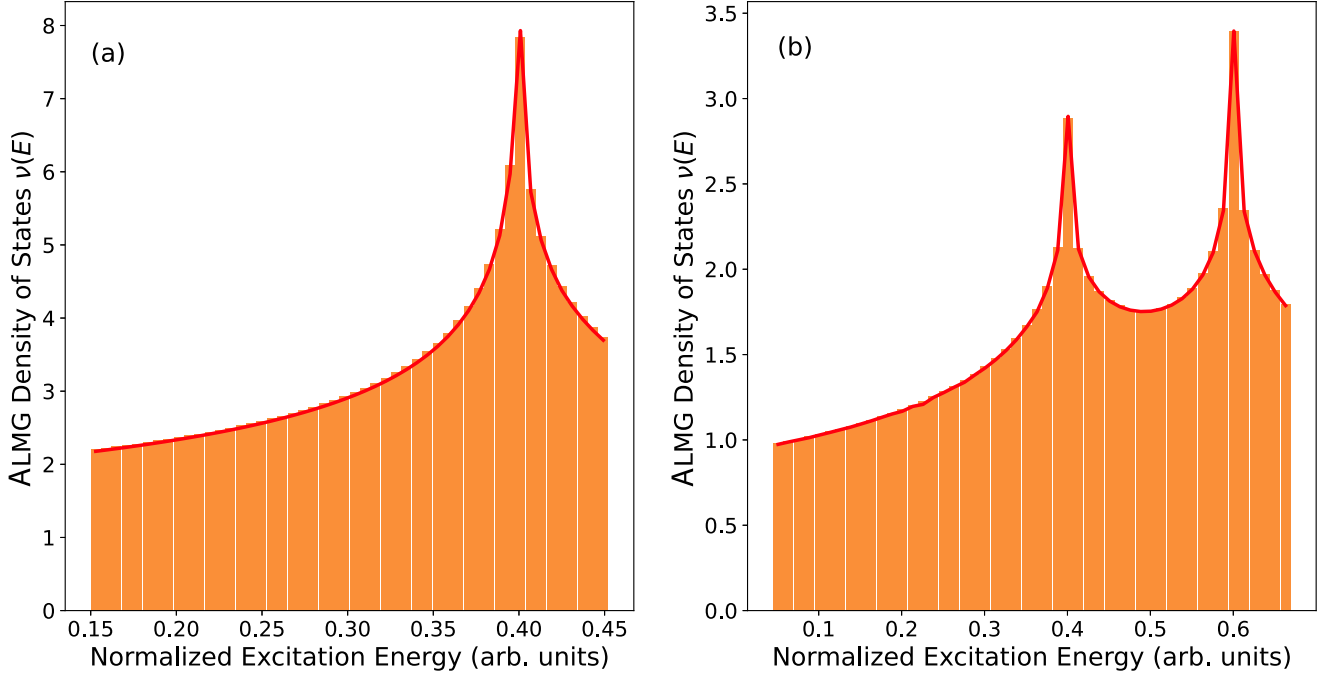


FIG. 4. Density of states $\nu(E)$ as a function of the normalized energy E/N for an ALMG Hamiltonian with $\alpha = -0.6$ and (a) $\xi = 0.15$ and (b) $\xi = 0.6$. The red solid line is the $\nu(E)$ density of states computed with Eq. (15). Also depicted is the density of states computed for the normalized eigenvalues of an ALMG Hamiltonian (3) with $N = 4000$ (orange bars).

where it is clear how the threshold value of α exists and is equal to the value $\alpha_{th}(\xi_c) = -0.4$.

As can be clearly seen in Fig. 1, the existence of an ESQPT can be traced back to abrupt changes in the system available phase space which produces a maximum in the local density of states at the separatrices, for the critical energy of the transition [12,24,31,48]. From the classical Hamiltonian (10), we can evaluate the semiclassical approximation to the quantum density of states as a function of the system’s energy [78]. In the particular case of the LMG and ALMG models

$$\begin{aligned} \nu(E) &= \frac{1}{2\pi} \iint dq dp \delta(E - H_{cl}(q, p)) \\ &= \frac{1}{2\pi} \iint d\phi dj_z \delta(E - H_{cl}(\phi, j_z)), \end{aligned} \quad (15)$$

where instead of the phase-space generalized coordinate and associated momentum we used a different pair of canonical variables $\phi \in [0, 2\pi)$ and $j_z \in [-j, j]$ that facilitate the derivation of an analytical formula for the density of states of the ALMG model. Using the properties of the Dirac delta function (see the Appendix), we can obtain the analytical formula for the density of states

$$\begin{aligned} \nu(\varepsilon) &= \frac{1}{4\pi} \int_0^{2\pi} d\phi \\ &\times \frac{1}{\sqrt{\left(\frac{1-\xi+\alpha}{2}\right)^2 - (\alpha + 4\xi \cos^2 \phi) \left(\frac{2+2\xi+\alpha}{4} - \xi \cos^2 \phi - \varepsilon\right)}}, \end{aligned} \quad (16)$$

where ε is the scaled energy value $\varepsilon = E/N$.

In Fig. 4 we plot the density of states $\nu(E)$ calculated with Eq. (16) (red line) versus the normalized energy for $\alpha = -0.6$ (the same α value used in the correlation energy diagrams of Fig. 1) and two ξ values: 0.15 [symmetric phase, Fig. 4(a)] and 0.6 [broken-symmetry phase, Fig. 4(b)]. For the sake of comparison, we also include the density of states computed from the eigenvalues of an ALMG Hamiltonian (3) for the same control parameters and a system size $N = 2000$. It can be clearly appreciated how the density of states in Fig. 4(a) has a maximum at the $f_2(\xi = 0.15, \alpha = -0.6) + E_{gs}(\xi = 0.15, \alpha = -0.6) = 0.4$ critical energy in the symmetric phase and in Fig. 4(b) at $f_1(\xi = 0.6, \alpha = -0.6) + E_{gs}(\xi = 0.6, \alpha = -0.6) = 0.4$ (leftmost maximum) and $f_2(\xi = 0.6, \alpha = -0.6) + E_{gs}(\xi = 0.6, \alpha = -0.6) = 0.6$ (rightmost maximum) critical energies in the broken-symmetry phase. The agreement between the results for Eq. (16) and the density of states computed from the system energies is excellent and it is worth noting how in all cases the peaks will transform into logarithmic divergences for an infinite system size, as expected [14]. This has deep implications in the system dynamics, as shown in [70].

In the next section we characterize the two ESQPTs and their associated separatrices using different quantities.

III. RESULTS

In this section we characterize the two ESQPTs that arise in the ALMG using four different quantities: the gap between adjacent positive-parity energy levels, the expectation value of the operator $\hat{n} = S + \hat{\mathcal{S}}_z$, the participation ratio, and the quantum fidelity susceptibility.

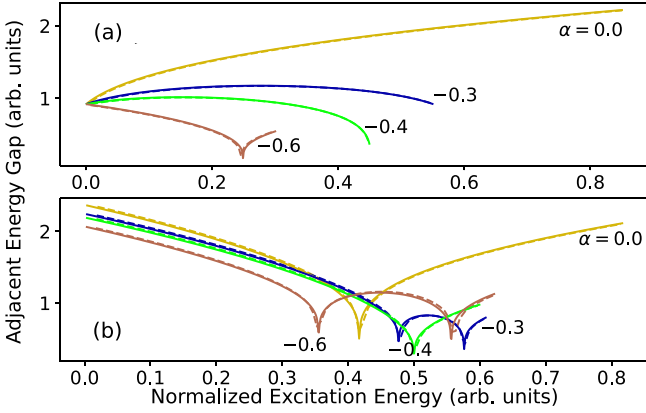


FIG. 5. Gap between adjacent energy levels in the ALMG model as a function of the normalized excitation energy for (a) $\xi = 0.15$ and (b) $\xi = 0.6$; anharmonicity parameter $\alpha = 0$ (yellow), -0.3 (blue), -0.4 (green), and -0.6 (brown); and system size $N = 120$ (dashed lines) and 1200 (solid lines).

A. Energy gap

The occurrence of an ESQPT is most often marked by a discontinuity in the density of states or one of its derivatives. In cases such as the LMG model (2), for a given value of the control parameter $\xi > \xi_c = 0.2$, the difference in energy between adjacent eigenstates is minimum at or close to the critical energy of the ESQPT, due to the high density of states at this excitation energy (see Fig. 1). Results are more complex once we introduce the anharmonic correction in the LMG model Hamiltonian (3).

In Fig. 5 we plot the difference between adjacent positive-parity energy levels as a function of the normalized excitation energy for system-size values $N = 2S = 120$ (dashed lines) and 1200 (solid lines), for control parameter ξ equal to 0.15 [Fig. 5(a)] and 0.6 [Fig. 5(b)], and for $\alpha = 0, -0.3, -0.4, -0.6$. The results in Fig. 5(a), where the system is in the symmetric phase ($\xi = 0.15 < \xi_c$), can be explained by considering the second separatrix (14). The $f_2(\xi, \alpha)$ line marks the critical energy value for the ESQPT associated with the anharmonic term in $\xi > \xi_c$ and, as explained above, there is a threshold α and the effects of the anharmonic term in this phase can be noticed only when the parameter α is beyond this threshold value [see the line for $\alpha = -0.4$ in Fig. 5(a)]. The crossing of the critical energy is marked by an abrupt minimum in the energy gap, as expected. When this study is extended to the broken-symmetry phase [Fig. 5(b)], there are two minima, one for each separatrix, for negative α values, except for $\alpha = -0.4$, as this corresponds to the point associated with the crossing of $f_1(\xi, \alpha)$ and $f_2(\xi, \alpha)$ in Fig. 1(b). As expected, the ESQPT precursor is better defined for larger system size, though for $N = 2S = 120$ the results already clearly identify the ESQPT. The ALMG energy gap results are in good agreement with the 2DVM results obtained in the symmetric [30] and broken-symmetry [29] cases.

B. Number operator

The $S + \hat{S}_z$ term in Eqs. (2) and (3) is associated with the $u(1)$ Casimir operator and it can be denoted by the system

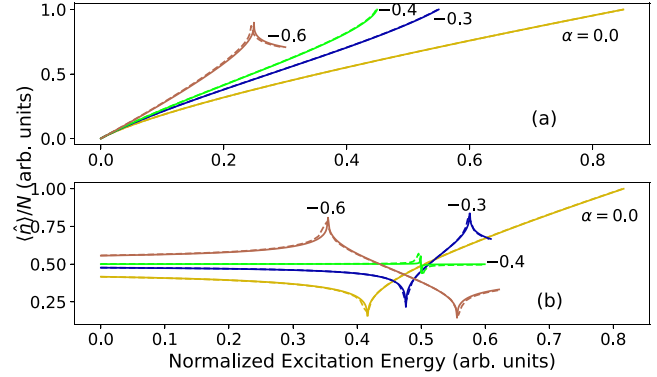


FIG. 6. Expectation value of the number operator \hat{n} in the system eigenstates for (a) $\xi = 0.15$ and (b) $\xi = 0.6$; anharmonicity parameter $\alpha = 0$ (yellow), -0.3 (blue), -0.4 (green), and -0.6 (brown); and system size $N = 120$ (dashed lines) and 1200 (solid lines).

number operator \hat{n} . This Casimir operator provides a suitable realization of an order parameter for the ground-state QPT in the ALMG case [35–37,47,51]. The expectation value of this operator in the system eigenstates is a second ESQPT proxy in the Hamiltonian (3). We depict in Fig. 6 the expectation value of \hat{n} as a function of the normalized system excitation energy for $\xi = 0.15$ [Fig. 6(a)] and 0.6 [Fig. 6(b)] and different values of the anharmonicity parameter α (see the figure caption) for system size $N = 120$ (dashed lines) and 1200 (solid lines). In all cases, the expectation value of \hat{n} is a well-defined minimum (maximum) for the eigenstates closer to the $f_1(\xi, \alpha)$ [$f_2(\xi, \alpha)$] separatrix. This fact will be better understood once we introduce the inverse participation ratio to characterize both ESQPTs.

It is worth emphasizing that in the symmetric case there is no minimum; the $f_1(\xi, \alpha)$ line is only defined for $\xi > \xi_c$. This is clearly shown in Fig. 6(a), where $\xi = 0.15 < \xi_c$. In addition, as in the energy gap case, this quantity has a peak only for values beyond the α threshold value that corresponds to the second separatrix $f_2(\xi, \alpha)$.

C. Participation ratio

The participation ratio (PR) provides the localization of a quantum state in a given basis [79]. For a state $|\psi\rangle$, expressed in a basis $\{|n\rangle\}_{n=0}^{D-1}$ as $|\psi\rangle = \sum_{n=0}^{D-1} C_n |n\rangle$, the PR is defined as

$$P(\psi) = \frac{1}{\sum_{n=0}^{D-1} |C_n|^4}, \quad (17)$$

where D stands for the Hilbert space dimension, which in this case is $D = N + 1$. This quantity is also often referred to as the inverse participation ratio [80] or the number of principal components [81]. In the case in which the state is maximally delocalized, $C_n = 1/\sqrt{D}$ for all n and $P(\psi) = D$; if the state is equal to one basis element (all $C_n = 0$ but one that is equal to unity), the localization is maximal in the basis and $P(\psi) = 1$. A series of works in algebraic models for systems in one-, two-, and three-dimensions having a $u(n+1)$ dynamical algebra has shown that the eigenstates closer to the critical energy in a $u(n) - so(n+1)$ second-order ground-state quantum phase transition are strongly localized in the

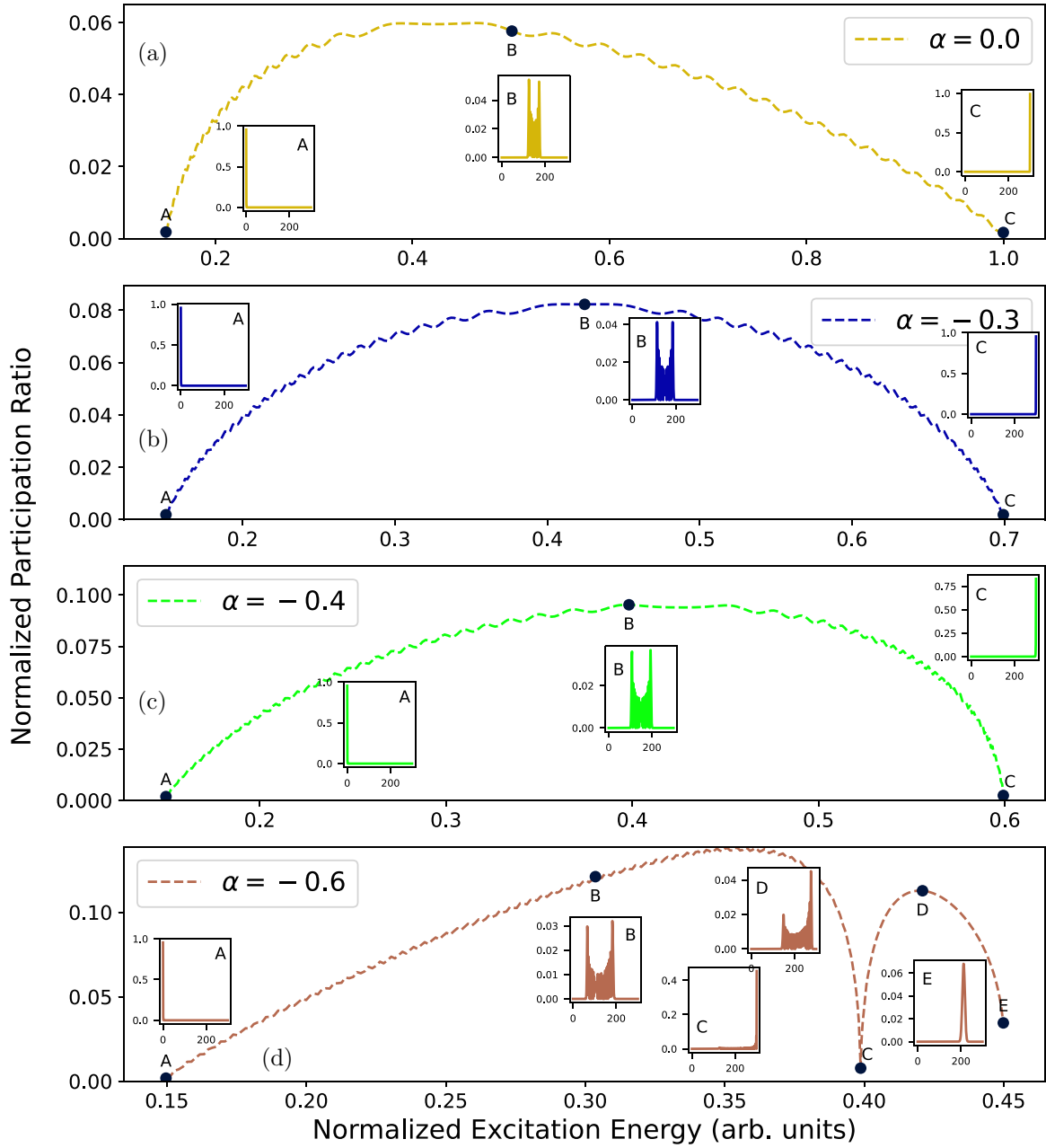


FIG. 7. Normalized participation ratio as a function of the normalized excitation energy for an ALMG model with $\xi = 0.15$, system size $N = 600$, and different anharmonicity parameter values: (a) $\alpha = 0$ (yellow), (b) $\alpha = -0.3$ (blue), (c) $\alpha = -0.4$ (green), and (d) $\alpha = -0.6$ (brown). In each case, the PR values for eigenstates of interest have been marked with black circles and the squared components of these eigenstates as a function of the corresponding $u(1)$ basis state index are shown in the insets (see the text for details).

$u(n)$ basis [51,82,83]. In the ALMG case there is a strong localization in the $u(1)$ basis of the states close to either one of the two separatrices. In particular, the eigenstates with energies close to the critical energy of the $f_1(\xi, \alpha)$ separatrix are highly localized in the $n = 0$ component ($|S, M_z = -S\rangle$) of the basis, something that was already checked in [51] for the LMG model. However, for the localization of the eigenstates with energies close to the second separatrix $f_2(\xi, \alpha)$, critical energy is due to a high component in the $n = N$ basis state ($|S, M_z = S\rangle$). This is shown in Figs. 7 and 8 for systems in the symmetric phase ($\xi = 0.15$) and in the broken-symmetry phase, respectively. In both cases, the system size is $N = 600$

and results are depicted for (from top to bottom) $\alpha = 0$, -0.3 , -0.4 , and -0.6 . In each panel some representative eigenstates have been chosen and the values of their squared components in the $u(1)$ basis are shown in the corresponding insets.

In Fig. 7 the only α value beyond the threshold value is $\alpha = -0.6$, shown in Fig. 7(d). In Figs. 7(a)–7(c) the PR is minimum at the spectrum edges, where eigenstates are maximally localized in the $|S, M_z = -S\rangle$ and $|S, M_z = S\rangle$ states, as expected in the symmetric phase where the $u(1)$ dynamical symmetry provides a convenient approximation. However, in Fig. 7(d) (brown line), a well-defined PR minimum appears

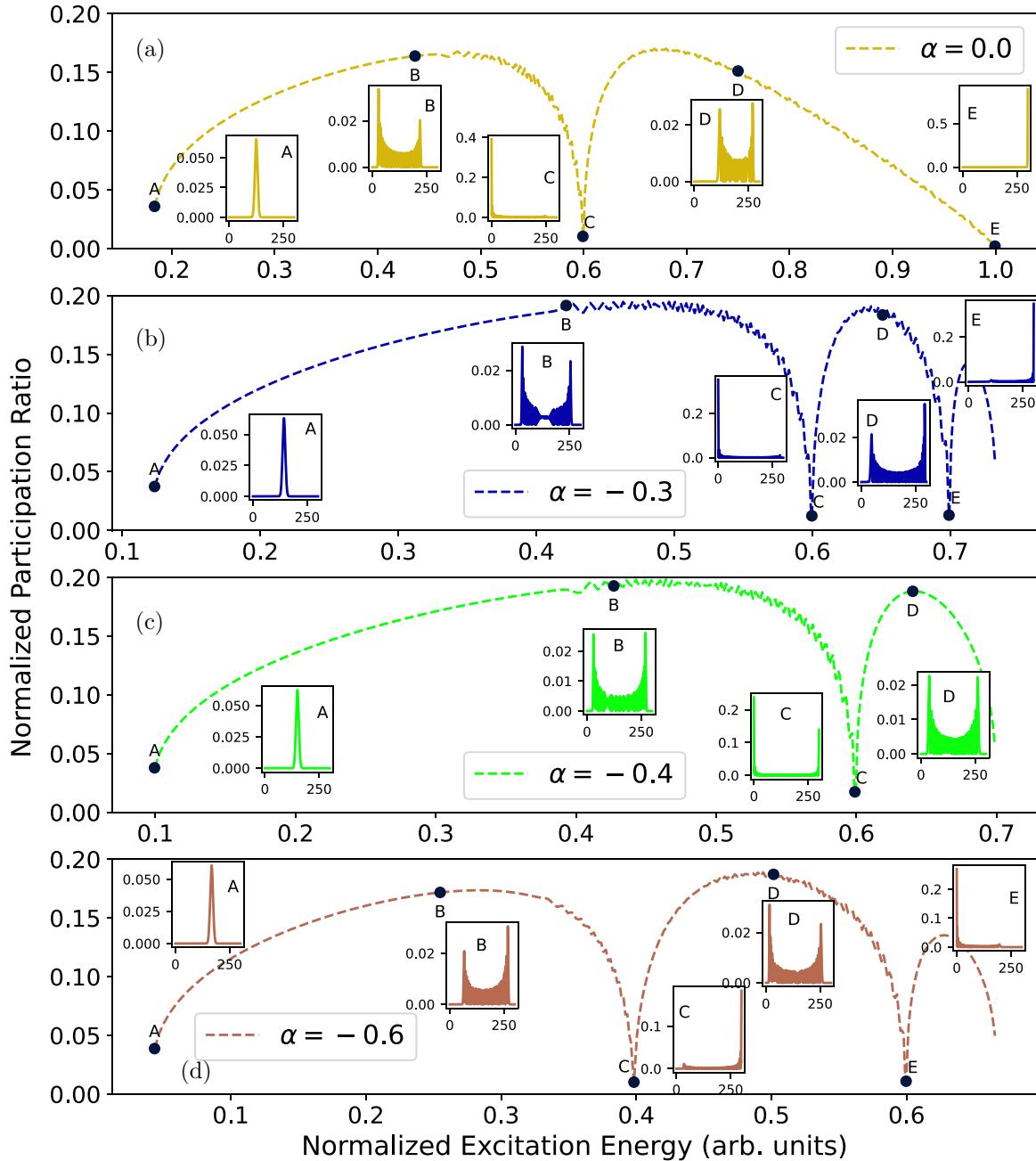


FIG. 8. Normalized participation ratio as a function of the normalized excitation energy for an ALMG model with $\xi = 0.6$, system size $N = 600$, and different anharmonicity parameter values: (a) $\alpha = 0$ (yellow), (b) $\alpha = -0.3$ (blue), (c) $\alpha = -0.4$ (green), and (d) $\alpha = -0.6$ (brown). In each case, the PR values for eigenstates of interest have been marked with black circles and the squared components of these eigenstates as a function of the corresponding $u(1)$ basis state index are shown in the insets (see the text for details).

associated with the $f_2(\xi, \alpha)$ separatrix and the ESQPT induced by the anharmonic term in Eq. (3). The eigenstate labeled as C in this panel, i.e., the eigenstate with a minimum PR value which is not in the spectrum edges, is highly localized (low PR) and its squared components in the inset reveal that the localization takes place for the last basis state $|S, M_z = S\rangle$.

The PR values in the broken-symmetry phase are shown in Fig. 8. In the $\alpha = 0$ case [Fig. 8(a), yellow curve], the states at the edge of the spectrum have low values of the

PR, as expected, and the ground state is not well localized in the $n = 0$ basis state, as we have straddled the critical ground-state QPT and the $u(1)$ dynamical symmetry is no longer a convenient approximation for the system eigenstates. There is a local PR minimum, labeled as C , associated with the $f_1(\xi, \alpha)$ separatrix and the ESQPT that stems from the appearance of a maximum in the origin. When $\alpha = -0.3$ [Fig. 8(b), blue curve], precursors from both ESQPTs can be observed. In this case the $f_1(\xi, \alpha)$ separatrix is found at lower energies than the $f_2(\xi, \alpha)$ separatrix and the states close to

the separatrices and that constitute local minima for the PR are labeled as C and E , respectively. Both states are strongly localized and, from the information in the insets, the first one has a dominant component in the $|S, M_z = -S\rangle$ basis state and the second case in the $|S, M_z = S\rangle$ basis state. The situation is reversed in the $\alpha = -0.6$ case [Fig. 8(d), brown curve] as the anharmonicity induced ESQPT (C state) lies now at lower energies than the original ESQPT (E state). Figure 8(c) (green curve) is a special case, where only one PR local minimum appears, besides the spectrum edges, as for these particular ξ and α values there is a crossing of the two separatrices. The eigenstate having a local minimum value of the PR, labeled as C , is well localized with high components in both $|S, M_z = -S\rangle$ and $|S, M_z = S\rangle$ basis states. This is in good agreement with the results obtained for an anharmonic 2DVM Hamiltonian [18,30].

D. Quantum fidelity susceptibility

Quantum fidelity for a system with a single control parameter λ and a Hamiltonian $\hat{H}(\lambda) = \hat{H}^0 + \lambda\hat{H}^I$ is defined as the modulus of the overlap between the ground state of the system for λ and $\lambda + \delta\lambda$,

$$F(\lambda, \delta\lambda) = |\langle \psi_0(\lambda) | \psi_0(\lambda + \delta\lambda) \rangle|. \quad (18)$$

This quantity, originally introduced in the realm of quantum information [84], was later used for the characterization of QPTs as it efficiently tracks the sudden change in the wave function of the system ground state as it straddles the critical value of the control parameter [85–87]. The quantum fidelity susceptibility (QFS) is defined as the second-order (and leading) term in the series expansion of $F(\lambda, \delta\lambda)$ as a function of $\delta\lambda$ [86,87],

$$\chi_F(\lambda) = -\frac{\partial^2 F(\lambda, \delta\lambda)}{\partial(\delta\lambda)^2} = \lim_{\delta\lambda \rightarrow 0} \frac{-2 \ln F(\lambda, \delta\lambda)}{(\delta\lambda)^2}. \quad (19)$$

The QFS reaches a maximum at the critical value of the λ control parameter and it is independent of the $\delta\lambda$ value. Using first-order perturbation theory, the QFS can be expressed as [87]

$$\chi_F(\lambda) = \sum_{i \neq 0}^{D-1} \frac{|\langle \psi_i(\lambda) | \hat{H}^I | \psi_0(\lambda) \rangle|^2}{[E_i(\lambda) - E_0(\lambda)]^2}, \quad (20)$$

where $|\psi_i(\lambda)\rangle$ is the i th eigenvector of the Hamiltonian $\hat{H}(\lambda)$ and $E_i(\lambda)$ is its associated eigenvalue.

Recently, Khalouf-Rivera *et al.* suggested to extend the use of the QFS to the study of ESQPTs using as an example the 2DVM and its application to the bending of nonrigid molecules [88]. Following the procedure detailed in that work, we define a Hamiltonian with a new control parameter $\lambda \in [-1, 1]$ grouping the interactions in Eq. (3) considering the dynamical symmetry they belong to

$$\begin{aligned} \hat{H}(\lambda) &= (1 - \lambda) \left\{ (1 - \xi)(S + \hat{S}_z) + \frac{\alpha}{2S}(S + \hat{S}_z)(S + \hat{S}_z + 1) \right\} \\ &+ (1 + \lambda) \left\{ \frac{2\xi}{S}(S^2 - \hat{S}_x^2) \right\}, \end{aligned} \quad (21)$$

$$\begin{aligned} \hat{H}(\lambda) &= \hat{H}_0 + \lambda\hat{H}^I, \\ \hat{H}^I &= -(1 - \xi)(S + \hat{S}_z) - \frac{\alpha}{2S}(S + \hat{S}_z)(S + \hat{S}_z + 1) \\ &+ \frac{2\xi}{S}(S^2 - \hat{S}_x^2). \end{aligned} \quad (22)$$

In this way, if our starting point is a Hamiltonian (3) with given values of ξ and α , the Hamiltonian (22) for $\lambda = -1$ ($\lambda = 1$) is diagonal in the $u(1)$ [so(2)] basis and we recover the original Hamiltonian for $\lambda = 0$. The QFS definition in Eq. (20) can be extended to encompass excited states of the Hamiltonian (22) [88],

$$\chi_F^{(j)}(\lambda) = \sum_{i \neq j}^{D-1} \frac{|\langle \psi_i(\lambda) | \hat{H}^I | \psi_j(\lambda) \rangle|^2}{[E_i(\lambda) - E_j(\lambda)]^2}, \quad (23)$$

where $|\psi_j(\lambda)\rangle$ is the j th eigenstate of the $\hat{H}(\lambda)$ Hamiltonian with $j = 0, \dots, D - 1$.

In Fig. 9(a) we report the normalized QFS χ/N^2 as a function of the normalized excitation energy E/N for the ALMG model with $\xi = 0.3$ and $\alpha = -0.6$, a system which is located between the ground-state QPT and the separatrices cross, and different system sizes $N = 256$ (blue), 512 (orange), 1024 (green), 2048 (red), and 4096 (purple). In both transitions the QFS is maximum near the critical energy, since the maximum due to f_1 (lower energy) is higher than the f_2 one (higher energy). In Figs. 9(b) and 9(c) we show a detailed close-up of peaks, i.e., the lower-energy transition [Fig. 9(b)] and higher-energy transition [Fig. 9(c)]. We have added an interpolation with splines for each system (red dashed lines) and highlighted its maximum value (red pluses). Therefore, the mean field values of the critical energies are plotted with black dotted lines. In Figs. 9(d) and 9(e) we plot the maximum value of QFS $\chi_{\text{spline}}^{\text{max}}$ (chartreuse circles and left axes) as well as its position with respect to the mean field value $|E_{\text{spline}}^{\text{max}}/N - f_{\text{MF}}|$ (black pluses and right axes) using logarithmic scale. As expected, in both transitions the critical energy tends to the mean field value and the QFS diverges according to power laws

$$\chi_{\text{spline}}^{\text{max}} \propto N^a, \quad (24)$$

$$|E_{\text{spline}}^{\text{max}}/N - f_{\text{MF}}| \propto N^b, \quad (25)$$

with $a = 2.110(7)$ and $b = -1.009(6)$ for the first transition (13) and $a = 2.125(4)$ and $b = -0.947(14)$ for the second transition (14).

IV. CONCLUSION

In this first work of a series of two papers (the second paper is Ref. [70]), we have analyzed the QPT and ESQPTs in the LMG model, including in the model Hamiltonian an anharmonic term dependent on the second-order Casimir operator of the $u(1)$ system subalgebra $(S + \hat{S}_z)(S + \hat{S}_z + 1)$. We have thoroughly studied this system with a focus on its static properties. The second work deals with dynamic aspects and how the ESQPTs modify the system evolution. This work has been fostered by the results obtained considering anharmonicity effects in the 2DVM, and the main motivation to extend this study to the LMG model is twofold. On the one

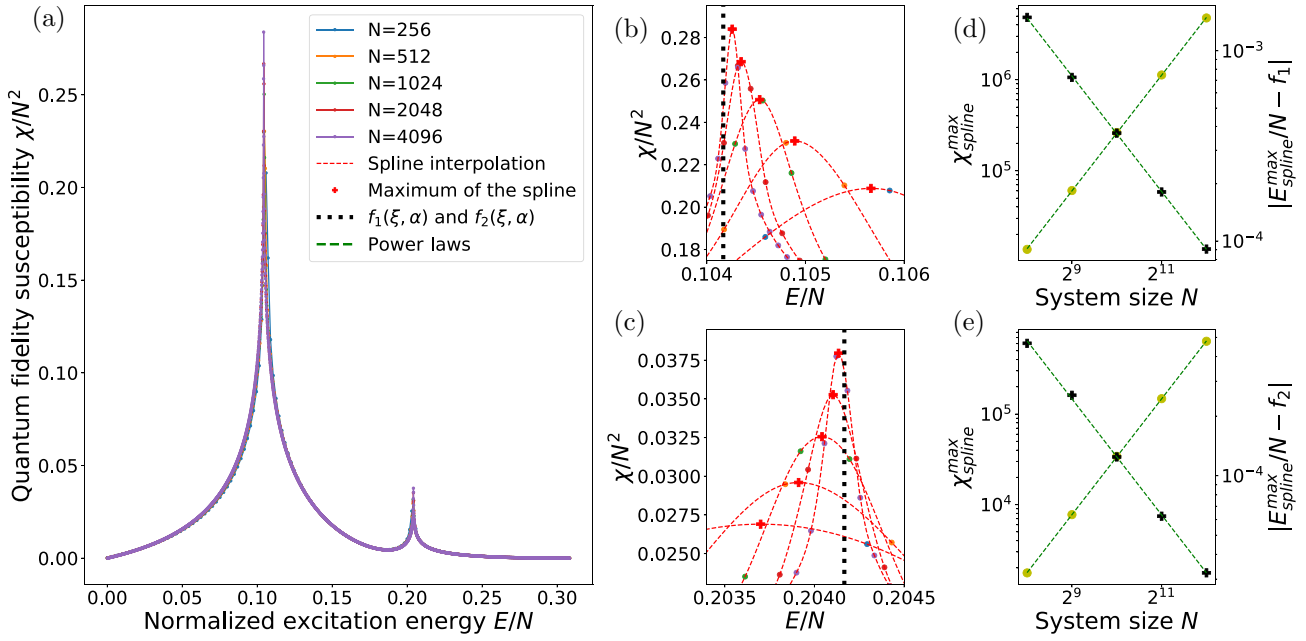


FIG. 9. (a) Normalized quantum fidelity susceptibility $\chi_F^{(j)}(\lambda = 0)/N^2$ as a function of the normalized excitation energy for the ALMG with $\xi = 0.3$ and $\alpha = -0.6$ for different system sizes $N = 256$ (blue), 512 (orange), 1024 (green), 2048 (red), and 4096 (purple). (b) and (c) Close-up of each extreme of the QFS. The mean field values of the critical energies (13) and (14) are plotted with a black dotted line. The red dashed lines correspond to the interpolation with splines used to locate the positions of maxima, which are highlighted with red pluses. (d) and (e) Maximum values obtained with the interpolation of the QFS $\chi_{\text{spline}}^{\text{max}}$ (chartreuse circles and left axes) and the distances of the energies where these maxima occur to the mean field critical energies $|E_{\text{spline}}^{\text{max}}/N - f_{\text{MF}}|$ (black pluses and right axes) versus the system size N using logarithmic scale. The power interpolation has been added (green dashed lines) in all cases. See the text for details.

hand, the test of different approaches in the LMG model has been pervasive since their definition in nuclear structure studies. It is a simple toy model that offers an excellent playground for approximations and theoretical studies. On the other hand, the possibility of accessing experimental realizations of the model provides further interest in studies based on the LMG model.

Apart from defining the ALMG model Hamiltonian and its mean field limit energy functional, we have presented the ground-state QPT properties for its energy functional as well as the two ESQPTs that appear in the system for negative values of the anharmonicity parameter α . The mean field results for the ground-state QPT properties do not qualitatively change under the inclusion of the anharmonic term in the model Hamiltonian. There are still two phases, a symmetric one and a broken-symmetry phase, with a critical value of the ξ control parameter $\xi_c = 0.2$ that marks a point where a second-order ground-state QPT takes place. The first ESQPT is linked to the ground-state QPT in the sense that it can be explained from the existence of a local maximum in the energy functional once the control parameter goes through its critical value and enters the system's broken-symmetry phase. However, the second ESQPT is explained from the influence of the anharmonic term on the phase-space boundary of the system, something that in the classical or mean field limit of the system is reflected as a lowering of the asymptotic values of the energy functional for negative values of the parameter α . The influence on the system's spectrum of the two ESQPTs can be seen in Fig. 1(b), where even- and odd-parity

states are shown: The level piling and different degeneracy patterns depending on the ESQPT phases are clearly shown, together with the two separatrices. We have deduced from the classical energy functional analytic expressions for the two separatrix lines $f_1(\xi, \alpha)$ and $f_2(\xi, \alpha)$, valid in the thermodynamical limit, and we have illustrated how there is a threshold value of the parameter α for the second ESQPT to be manifested in the symmetric phase of the system, for $\xi < \xi_c$ (see Fig. 3).

We have characterized the ALMG ESQPTs computing the adjacent energy level gap, the expectation value of the $u(1)$ number operator, the participation ratio, and the quantum fidelity susceptibility for various values of the anharmonicity parameter and system sizes. The calculations were carried out for two values of the control parameter ξ : $\xi = 0.15$ for a system in the symmetric phase and $\xi = 0.6$, which brings the system into the broken-symmetry phase. The quantities we have used allow us to clearly locate both ESQPTs, and the PR shows a strong localization for states with energies close to the critical ESQPT energies. In the ESQPT with separatrix $f_1(\xi, \alpha)$, the localization happens for the $|S, -S\rangle$ basis state, while for the second ESQPT, with separatrix $f_2(\xi, \alpha)$, the localization occurs in the $|S, S\rangle$ basis state. The QFS is also sensitive to both ESQPTs, having a larger impact on the QFS value, with the ESQPT occurring at lower energies.

The existence of ESQPTs has strong implications on system structure and dynamics. Recently, it was proposed that a conserved quantity can be defined in one of the phases of an

ESQPT and the equilibrium values of relevant observables in this phase are dependent on the value of this newly defined constant [89]. This important result can be applied to the ESQPTs with separatrices $f_1(\xi, \alpha)$ and $f_2(\xi, \alpha)$. Exploring this issue will be a future development of interest with the ALMG.

ACKNOWLEDGMENTS

The authors thank José Enrique García Ramos and Miguel Carvajal Zaera for fruitful and inspiring discussions on the topic of this paper. This work is part of the $I + D + i$ Projects No. PID2019-104002GB-C21, No. PID2019-104002GB-C22, and No. PID2020-114687GB-I00 funded by Grant No. MCIN/AEI/10.13039/501100011033. This work was also partially supported by the Consejería de Conocimiento, Investigación y Universidad, Junta de Andalucía and European Regional Development Fund (ERDF), Grants No. UHU-1262561 and No. US-1380840 and it is also part of grant groups FQM-160 and FQM-287 and the project PAIDI 2020 Project No. P20_01247, funded by the Consejería de Economía, Conocimiento, Empresas y Universidad, Junta de Andalucía (Spain) and ERDF—A Way of Making Europe, by the European Union or by the European Union NextGenerationEU/PRTR. Computing resources supporting this work were provided by the CEAFCM and Universidad de Huelva High Performance Computer located in the Campus Universitario el Carmen and funded by FEDER/MINECO Project No. UNHU-15CE-2848.

APPENDIX: ALMG MODEL DENSITY OF STATES

As mentioned in the main text, when obtaining the density of states for the ALMG model using the Gutzwiller semiclassical approximation [78], it is handier to recast the ALMG Hamiltonian by replacing the pseudospin \hat{S}_i with a classical angular momentum j_i , instead of the q and p generalized

coordinate and momentum used in Eq. (10),

$$H_{cl} = (1 - \xi)(j + j_z) + \frac{\alpha}{2j}(j + j_z)(j + j_z + 1) + \frac{2\xi}{j}(j^2 - j_z^2). \tag{A1}$$

We introduce the classical angular momentum azimuthal angle $\phi = \tan^{-1}(j_y/j_x) \in [0, 2\pi)$ and its z component $j_z \in [-j, j]$ as a valid pair of canonical variables

$$H_{cl} = (1 - \xi)(j + j_z) + \frac{\alpha}{2j}(j + j_z)(j + j_z + 1) + \frac{2\xi}{j}[j^2 - (j^2 - j_z^2) \cos^2 \phi]. \tag{A2}$$

The density of states (15) for the new pair of canonical variables is

$$\nu(E) = \frac{1}{2\pi} \int_0^{2\pi} d\phi \int_{-j}^j dj_z \delta(E - H_{cl}(\phi, j_z)) = \frac{1}{2\pi} \frac{N}{2} \int_0^{2\pi} d\phi \int_{-1}^1 dx \delta(E - H_{cl}(\phi, x)), \tag{A3}$$

where we introduce the rescaled variable $x = j_z/j \in [-1, 1]$ and the corresponding Jacobian term $j = N/2$. Working, as in Eq. (7), with the Hamiltonian and energy per particle $\mathcal{H} = H_{cl}/N$ and $\varepsilon = E/N$ and taking into consideration the Dirac delta property $\int dz \delta(z/a) = |a| \int dz \delta(z)$, we obtain

$$\nu(\varepsilon) = \frac{1}{4\pi} \int_0^{2\pi} d\phi \int_{-1}^1 dx \delta(\varepsilon - \mathcal{H}(\phi, x)). \tag{A4}$$

In order to continue, the Dirac delta composition with a function $f(x)$ is

$$\delta(f(x)) = \sum_i \frac{\delta(x - x_i)}{\left| \frac{df(x_i)}{dx} \right|}, \tag{A5}$$

where the sum extends over all x_i , the different roots of $f(x)$. If we apply this property to $f(x) = \varepsilon - \mathcal{H}(\phi, x)$ in Eq. (A4) we have two possible roots

$$x_{\pm} = \frac{\xi - 1 - \alpha \pm \sqrt{(1 - \xi + \alpha)^2 - (\alpha + 4\xi \cos^2 \phi)(2 + 2\xi + \alpha - 4\xi \cos^2 \phi - 4\varepsilon)}}{\alpha + 4\xi \cos^2 \phi}, \tag{A6}$$

though x_- is not a valid solution as it is outside the x variable range. Applying Eq. (A5) to Eq. (A4) for the x_+ root, we obtain the final result in Eq. (16),

$$\nu(\varepsilon) = \frac{1}{4\pi} \int_0^{2\pi} d\phi \frac{1}{\left| \sqrt{\left(\frac{1-\xi+\alpha}{2}\right)^2 - (\alpha + 4\xi \cos^2 \phi)\left(\frac{1+\xi}{2} + \frac{\alpha}{4} - \xi \cos^2 \phi - \varepsilon\right)} \right|}. \tag{A7}$$

[1] L. Carr, *Understanding Quantum Phase Transitions* (CRC, Boca Raton, 2010).
 [2] R. Gilmore and D. H. Feng, Phase transitions in nuclear matter described by pseudospin Hamiltonians, *Nucl. Phys. A* **301**, 189 (1978).
 [3] R. Gilmore, The classical limit of quantum nonspin systems, *J. Math. Phys.* **20**, 891 (1979).
 [4] D. H. Feng, R. Gilmore, and S. R. Deans, Phase transitions and the geometric properties of the interacting boson model, *Phys. Rev. C* **23**, 1254 (1981).
 [5] P. Cejnar and J. Jolie, Quantum phase transitions in the interacting boson model, *Prog. Part. Nucl. Phys.* **62**, 210 (2009).
 [6] R. F. Casten, Quantum phase transitions and structural evolution in nuclei, *Prog. Part. Nucl. Phys.* **62**, 183 (2009).

- [7] P. Cejnar, J. Jolie, and R. F. Casten, Quantum phase transitions in the shapes of atomic nuclei, *Rev. Mod. Phys.* **82**, 2155 (2010).
- [8] P. Cejnar and F. Iachello, Phase structure of interacting boson models in arbitrary dimension, *J. Phys. A: Math. Theor.* **40**, 581 (2007).
- [9] P. Cejnar, M. Macek, S. Heinze, J. Jolie, and J. Dobeš, Monodromy and excited-state quantum phase transitions in integrable systems: Collective vibrations of nuclei, *J. Phys. A: Math. Gen.* **39**, L515 (2006).
- [10] M. A. Caprio, P. Cejnar, and F. Iachello, Excited state quantum phase transitions in many-body systems, *Ann. Phys. (NY)* **323**, 1106 (2008).
- [11] P. Cejnar and P. Stránský, Impact of quantum phase transitions on excited-level dynamics, *Phys. Rev. E* **78**, 031130 (2008).
- [12] P. Stránský, M. Macek, and P. Cejnar, Excited-state quantum phase transitions in systems with two degrees of freedom: Level density, level dynamics, thermal properties, *Ann. Phys. (NY)* **345**, 73 (2014).
- [13] P. Stránský, M. Macek, A. Leviatan, and P. Cejnar, Excited-state quantum phase transitions in systems with two degrees of freedom: II. Finite-size effects, *Ann. Phys. (NY)* **356**, 57 (2015).
- [14] P. Stránský and P. Cejnar, Classification of excited-state quantum phase transitions for arbitrary number of degrees of freedom, *Phys. Lett. A* **380**, 2637 (2016).
- [15] M. Macek, P. Stránský, A. Leviatan, and P. Cejnar, Excited-state quantum phase transitions in systems with two degrees of freedom. III. Interacting boson systems, *Phys. Rev. C* **99**, 064323 (2019).
- [16] D. Larese and F. Iachello, A study of quantum phase transitions and quantum monodromy in the bending motion of non-rigid molecules, *J. Mol. Struct.* **1006**, 611 (2011).
- [17] D. Larese, F. Pérez-Bernal, and F. Iachello, Signatures of quantum phase transitions and excited state quantum phase transitions in the vibrational bending dynamics of triatomic molecules, *J. Mol. Struct.* **1051**, 310 (2013).
- [18] J. Khalouf-Rivera, M. Carvajal, L. F. Santos, and F. Pérez-Bernal, Calculation of transition state energies in the HCN-HNC isomerization with an algebraic model, *J. Phys. Chem. A* **123**, 9544 (2019).
- [19] J. Khalouf-Rivera, F. Pérez-Bernal, and M. Carvajal, Excited state quantum phase transitions in the bending spectra of molecules, *J. Quant. Spectrosc. Radiat. Transfer* **261**, 107436 (2021).
- [20] B. Dietz, F. Iachello, M. Miski-Oglu, N. Pietralla, A. Richter, L. von Smekal, and J. Wambach, Lifshitz and excited-state quantum phase transitions in microwave Dirac billiards, *Phys. Rev. B* **88**, 104101 (2013).
- [21] L. Zhao, J. Jiang, T. Tang, M. Webb, and Y. Liu, Dynamics in spinor condensates tuned by a microwave dressing field, *Phys. Rev. A* **89**, 023608 (2014).
- [22] P. Feldmann, C. Klempt, A. Smerzi, L. Santos, and M. Gessner, Interferometric Order Parameter for Excited-State Quantum Phase Transitions in Bose-Einstein Condensates, *Phys. Rev. Lett.* **126**, 230602 (2021).
- [23] J. Cabedo, J. Claramunt, and A. Celi, Dynamical preparation of stripe states in spin-orbit-coupled gases, *Phys. Rev. A* **104**, L031305 (2021).
- [24] P. Cejnar, P. Stránský, M. Macek, and M. Kloc, Excited-state quantum phase transitions, *J. Phys. A: Math. Theor.* **54**, 133001 (2021).
- [25] F. Iachello and S. Oss, Algebraic approach to molecular spectra: Two dimensional problems, *J. Chem. Phys.* **104**, 6956 (1996).
- [26] F. Pérez-Bernal and F. Iachello, Algebraic approach to two-dimensional systems: Shape phase transitions, monodromy, and thermodynamic quantities, *Phys. Rev. A* **77**, 032115 (2008).
- [27] F. Iachello, F. Pérez-Bernal, and P. H. Vaccaro, A novel algebraic scheme for describing nonrigid molecules, *Chem. Phys. Lett.* **375**, 309 (2003).
- [28] F. Pérez-Bernal, L. F. Santos, P. H. Vaccaro, and F. Iachello, Spectroscopic signatures of nonrigidity: Algebraic analyses of infrared and Raman transitions in nonrigid species, *Chem. Phys. Lett.* **414**, 398 (2005).
- [29] F. Pérez-Bernal and O. Álvarez-Bajo, Anharmonicity effects in the bosonic U(2)-SO(3) excited-state quantum phase transition, *Phys. Rev. A* **81**, 050101(R) (2010).
- [30] J. Khalouf-Rivera, F. Pérez-Bernal, and M. Carvajal, Anharmonicity-induced excited-state quantum phase transition in the symmetric phase of the two-dimensional limit of the vibron model, *Phys. Rev. A* **105**, 032215 (2022).
- [31] M. A. Bastarrachea-Magnani, S. Lerma-Hernández, and J. G. Hirsch, Comparative quantum and semiclassical analysis of atom-field systems. I. Density of states and excited-state quantum phase transitions, *Phys. Rev. A* **89**, 032101 (2014).
- [32] H. J. Lipkin, N. Meshkov, and A. J. Glick, Validity of many-body approximation methods for a solvable model, *Nucl. Phys.* **62**, 188 (1965).
- [33] N. Meshkov, A. J. Glick, and H. J. Lipkin, Validity of many-body approximation methods for a solvable model: (II). Linearization procedures, *Nucl. Phys.* **62**, 199 (1965).
- [34] A. J. Glick, H. J. Lipkin, and N. Meshkov, Validity of many-body approximation methods for a solvable model: (III). Diagram summations, *Nucl. Phys.* **62**, 211 (1965).
- [35] R. Botet and R. Jullien, Large-size critical behavior of infinitely coordinated systems, *Phys. Rev. B* **28**, 3955 (1983).
- [36] S. Dusuel and J. Vidal, Finite-Size Scaling Exponents of the Lipkin-Meshkov-Glick Model, *Phys. Rev. Lett.* **93**, 237204 (2004).
- [37] S. Dusuel and J. Vidal, Continuous unitary transformations and finite-size scaling exponents in the Lipkin-Meshkov-Glick model, *Phys. Rev. B* **71**, 224420 (2005).
- [38] W. D. Heiss, F. G. Scholtz, and H. B. Geyer, The large N behaviour of the Lipkin model and exceptional points, *J. Phys. A: Math. Gen.* **38**, 1843 (2005).
- [39] F. Leyvraz and W. D. Heiss, Large- n Scaling Behavior of the Lipkin-Meshkov-Glick Model, *Phys. Rev. Lett.* **95**, 050402 (2005).
- [40] O. Castaños, R. López-Peña, J. G. Hirsch, and E. López-Moreno, Phase transitions and accidental degeneracy in nonlinear spin systems, *Phys. Rev. B* **72**, 012406 (2005).
- [41] O. Castaños, R. López-Peña, J. G. Hirsch, and E. López-Moreno, Classical and quantum phase transitions in the Lipkin-Meshkov-Glick model, *Phys. Rev. B* **74**, 104118 (2006).
- [42] G. Engelhardt, V. M. Bastidas, C. Emary, and T. Brandes, ac-driven quantum phase transition in the Lipkin-Meshkov-Glick model, *Phys. Rev. E* **87**, 052110 (2013).
- [43] E. Romera, M. Calixto, and O. Castaños, Phase space analysis of first-, second- and third-order quantum phase transitions in the Lipkin-Meshkov-Glick model, *Phys. Scr.* **89**, 095103 (2014).

- [44] S. Campbell, Criticality revealed through quench dynamics in the Lipkin-Meshkov-Glick model, *Phys. Rev. B* **94**, 184403 (2016).
- [45] M. Heyl, F. Pollmann, and B. Dóra, Detecting Equilibrium and Dynamical Quantum Phase Transitions in Ising Chains Via Out-of-Time-Ordered Correlators, *Phys. Rev. Lett.* **121**, 016801 (2018).
- [46] A. Relaño, J. M. Arias, J. Dukelsky, J. E. García-Ramos, and P. Pérez-Fernández, Decoherence as a signature of an excited-state quantum phase transition, *Phys. Rev. A* **78**, 060102(R) (2008).
- [47] P. Ribeiro, J. Vidal, and R. Mosseri, Exact spectrum of the Lipkin-Meshkov-Glick model in the thermodynamic limit and finite-size corrections, *Phys. Rev. E* **78**, 021106 (2008).
- [48] P. Pérez-Fernández, A. Relaño, J. M. Arias, J. Dukelsky, and J. E. García-Ramos, Decoherence due to an excited-state quantum phase transition in a two-level boson model, *Phys. Rev. A* **80**, 032111 (2009).
- [49] P. Pérez-Fernández, P. Cejnar, J. M. Arias, J. Dukelsky, J. E. García-Ramos, and A. Relaño, Quantum quench influenced by an excited-state phase transition, *Phys. Rev. A* **83**, 033802 (2011).
- [50] Z.-G. Yuan, P. Zhang, S.-S. Li, J. Jing, and L.-B. Kong, Scaling of the Berry phase close to the excited-state quantum phase transition in the Lipkin model, *Phys. Rev. A* **85**, 044102 (2012).
- [51] L. F. Santos, M. Távora, and F. Pérez-Bernal, Excited-state quantum phase transitions in many-body systems with infinite-range interaction: Localization, dynamics, and bifurcation, *Phys. Rev. A* **94**, 012113 (2016).
- [52] Q. Wang and F. Pérez-Bernal, Excited-state quantum phase transition and the quantum-speed-limit time, *Phys. Rev. A* **100**, 022118 (2019).
- [53] Q. Wang and F. Pérez-Bernal, Probing an excited-state quantum phase transition in a quantum many-body system via an out-of-time-order correlator, *Phys. Rev. A* **100**, 062113 (2019).
- [54] D. Gutiérrez-Ruiz, D. Gonzalez, J. Chávez-Carlos, J. G. Hirsch, and J. D. Vergara, Quantum geometric tensor and quantum phase transitions in the Lipkin-Meshkov-Glick model, *Phys. Rev. B* **103**, 174104 (2021).
- [55] D. J. Nader, C. A. González-Rodríguez, and S. Lerma-Hernández, Avoided crossings and dynamical tunneling close to excited-state quantum phase transitions, *Phys. Rev. E* **104**, 064116 (2021).
- [56] J. Vidal, J. M. Arias, J. Dukelsky, and J. E. García-Ramos, Scalar two-level boson model to study the interacting boson model phase diagram in the Casten triangle, *Phys. Rev. C* **73**, 054305 (2006).
- [57] J. E. García-Ramos, P. Pérez-Fernández, J. M. Arias, and E. Freire, Phase diagram of the two-fluid Lipkin model: A “butterfly” catastrophe, *Phys. Rev. C* **93**, 034336 (2016).
- [58] J. E. García-Ramos, P. Pérez-Fernández, and J. M. Arias, Excited-state quantum phase transitions in a two-fluid Lipkin model, *Phys. Rev. C* **95**, 054326 (2017).
- [59] J. Larson, Circuit QED scheme for the realization of the Lipkin-Meshkov-Glick model, *Europhys. Lett.* **90**, 54001 (2010).
- [60] M. J. Cervia, A. B. Balantekin, S. N. Coppersmith, C. W. Johnson, P. J. Love, C. Poole, K. Robbins, and M. Saffman, Lipkin model on a quantum computer, *Phys. Rev. C* **104**, 024305 (2021).
- [61] K. Chinni, P. M. Poggi, and I. H. Deutsch, Effect of chaos on the simulation of quantum critical phenomena in analog quantum simulators, *Phys. Rev. Res.* **3**, 033145 (2021).
- [62] C. F. Hirjibehedin, C.-Y. Lin, A. F. Otte, M. Ternes, C. P. Lutz, B. A. Jones, and A. J. Heinrich, Large magnetic anisotropy of a single atomic spin embedded in a surface molecular network, *Science* **317**, 1199 (2007).
- [63] S. Morrison and A. S. Parkins, Dynamical Quantum Phase Transitions in the Dissipative Lipkin-Meshkov-Glick Model with Proposed Realization in Optical Cavity QED, *Phys. Rev. Lett.* **100**, 040403 (2008).
- [64] T. Zibold, E. Nicklas, C. Gross, and M. K. Oberthaler, Classical Bifurcation at the Transition from Rabi to Josephson Dynamics, *Phys. Rev. Lett.* **105**, 204101 (2010).
- [65] A. G. Araujo-Ferreira, R. Auccaise, R. S. Sarthour, I. S. Oliveira, T. J. Bonagamba, and I. Roditi, Classical bifurcation in a quadrupolar NMR system, *Phys. Rev. A* **87**, 053605 (2013).
- [66] P. Jurcevic, B. Lanyon, P. Hauke *et al.*, Quasiparticle engineering and entanglement propagation in a quantum many-body system, *Nature (London)* **511**, 202 (2014).
- [67] P. Jurcevic, H. Shen, P. Hauke, C. Maier, T. Brydges, C. Hempel, B. P. Lanyon, M. Heyl, R. Blatt, and C. F. Roos, Direct Observation of Dynamical Quantum Phase Transitions in an Interacting Many-Body System, *Phys. Rev. Lett.* **119**, 080501 (2017).
- [68] J. A. Muniz, D. Barberena, R. J. Lewis-Swan, D. J. Young, J. R. K. Cline, A. M. Rey, and J. K. Thompson, Exploring dynamical phase transitions with cold atoms in an optical cavity, *Nature (London)* **580**, 602 (2020).
- [69] V. Makhalov, T. Satoor, A. Evrard, T. Chalopin, R. Lopes, and S. Nascimbene, Probing Quantum Criticality and Symmetry Breaking at the Microscopic Level, *Phys. Rev. Lett.* **123**, 120601 (2019).
- [70] J. Khalouf-Rivera, J. Gamito, F. Pérez-Bernal, J. M. Arias, and P. Pérez-Fernández, Excited-state quantum phase transitions in the anharmonic Lipkin-Meshkov-Glick model II: Dynamic aspects, [arXiv:2207.04489](https://arxiv.org/abs/2207.04489).
- [71] P. Richerme, Z.-X. Gong, A. Lee, C. Senko, J. Smith, M. Foss-Feig, S. Michalakis, A. V. Gorshkov, and C. Monroe, Non-local propagation of correlations in quantum systems with long-range interactions, *Nature (London)* **511**, 198 (2014).
- [72] A. Frank and P. Van Isacker, *Algebraic Methods in Molecular and Nuclear Structure Physics* (Wiley, New York, 1994).
- [73] L. Fortunato and L. Sartori, Detailed Analysis of Quantum Phase Transitions Within the $u(2)$ Algebra, *Commun. Theor. Phys.* **54**, 589 (2010).
- [74] J. M. Radcliffe, Some properties of coherent spin states, *J. Phys. A: Gen. Phys.* **4**, 313 (1971).
- [75] A. Relaño, C. Esebbag, and J. Dukelsky, Excited-state quantum phase transitions in the two-spin elliptic Gaudin model, *Phys. Rev. E* **94**, 052110 (2016).
- [76] P. Stránský, P. Cejnar, and R. Filip, Stabilization of product states and excited-state quantum phase transitions in a coupled qubit-field system, *Phys. Rev. A* **104**, 053722 (2021).

- [77] Á. L. Corps and A. Relaño, Energy cat states induced by a parity-breaking excited-state quantum phase transition, *Phys. Rev. A* **105**, 052204 (2022).
- [78] M. C. Gutzwiller, *Chaos in Classical and Quantum Mechanics* (Springer, New York, 2013).
- [79] F. M. Izrailev, Simple models of quantum chaos: Spectrum and eigenfunctions, *Phys. Rep.* **196**, 299 (1990).
- [80] F. Evers and A. D. Mirlin, Anderson transitions, *Rev. Mod. Phys.* **80**, 1355 (2008).
- [81] V. Zelevinsky, B. A. Brown, N. Frazier, and M. Horoi, The nuclear shell model as a testing ground for many-body quantum chaos, *Phys. Rep.* **276**, 85 (1996).
- [82] L. F. Santos and F. Pérez-Bernal, Structure of eigenstates and quench dynamics at an excited-state quantum phase transition, *Phys. Rev. A* **92**, 050101(R) (2015).
- [83] F. Pérez-Bernal and L. F. Santos, Effects of excited state quantum phase transitions on system dynamics, *Prog. Phys. Fortschr. Phys.* **65**, 1600035 (2017).
- [84] M. A. Nielsen and I. L. Chuang, *Quantum Computation and Quantum Information*, 10th ed. (Cambridge University Press, New York, 2011).
- [85] P. Zanardi and N. Paunković, Ground state overlap and quantum phase transitions, *Phys. Rev. E* **74**, 031123 (2006).
- [86] W.-L. You, Y.-W. Li, and S.-J. Gu, Fidelity, dynamic structure factor, and susceptibility in critical phenomena, *Phys. Rev. E* **76**, 022101 (2007).
- [87] S.-J. Gu, Fidelity approach to quantum phase transitions, *Int. J. Mod. Phys. B* **24**, 4371 (2010).
- [88] J. Khalouf-Rivera, M. Carvajal, and F. Pérez-Bernal, Quantum fidelity susceptibility in excited state quantum phase transitions: application to the bending spectra of nonrigid molecules, *SciPost Phys.* **12**, 002 (2022).
- [89] Á. L. Corps and A. Relaño, Constant of Motion Identifying Excited-State Quantum Phases, *Phys. Rev. Lett.* **127**, 130602 (2021).